VII

Publication VII

V. Hynönen, T. Kurki-Suonio, W. Suttrop, A. Stäbler, and ASDEX Upgrade Team (2008). Effect of radial electric field and ripple on edge neutral beam ion distribution in ASDEX Upgrade. *Plasma Physics and Controlled Fusion*[†] **50**(3) 035014 (15 pp).

[†] http://www.iop.org/journals/PPCF

IOP PUBLISHING PLASMA PHYSICS AND CONTROLLED FUSION

Plasma Phys. Control. Fusion **50** (2008) 035014 (15pp) doi:10.1088/0741-3335/50/3/035014

Effect of radial electric field and ripple on edge neutral beam ion distribution in ASDEX Upgrade

V Hynönen[1], T Kurki-Suonio[1], W Suttrop[2], A Stäbler[2] and the ASDEX Upgrade Team[2]

[1] Helsinki University of Technology, Association Euratom-TEKES, FI-02015 TKK, Finland
[2] Max-Planck-Institut für Plasmaphysik, Euratom Association, D-85740 Garching, Germany

E-mail: ville.hynonen@tkk.fi

Received 15 October 2007, in final form 24 January 2008
Published 18 February 2008
Online at stacks.iop.org/PPCF/50/035014

Abstract

The neutral beam injected fast ion distribution at the ASDEX Upgrade edge region is studied focusing on the difference between co- and counter-injected neutral beams. The slowing-down distribution of beam ions is simulated using the orbit-following Monte Carlo code ASCOT. The edge fast ion density and its gradient are higher for counter-injection than for co-injection. Also the distribution in the velocity space is different: for co-injection, there exists a population of untrapped particles which for counter-injection is found only when the effect of a non-constant, experimentally obtained quiescent H-mode radial electric field is included in the simulation. Toroidal ripple removes ions having small particle pitch, thereby reducing the density and density gradient, whereas the radial electric field has the opposite effect. Including simultaneously the effects of both ripple and the radial electric field restores the distribution close to the ideal case where both of them are neglected. The radial electric field is found to squeeze the orbit of a counter-injected neutral beam ion but to widen the orbit of a co-injected ion, and to cause transitions in the orbit topologies which are reflected in the fast ion distribution.

1. Introduction

Edge localized modes (ELMs), violent bursts of energy and particles, are characteristic of the high-confinement mode (H-mode). On the one hand, they can cause unacceptable heat loads onto the plasma-facing components, but on the other hand, they play an essential role controlling the density and impurities. A viable option for the H-mode is the so-called quiescent H-mode (QH-mode) in which the ELMs are replaced by more continuous, benign MHD activity called edge harmonic oscillations (EHO) [1]. The QH-mode was originally discovered in DIII-D in 1999 [2], and has thereafter been reproduced at ASDEX Upgrade [3] and JET [1]. So far, however, the QH-mode has been obtained only with counter-current neutral beam

injection (NBI) which is not necessarily acceptable especially with metal walls envisaged for future reactors. Moreover, the regular H-mode can be achieved with both injection directions. Therefore, counter-injection apparently is a necessary but not a sufficient condition for the QH-mode. Finding out the trigger for the EHO-operation has proved elusive, but since counter-injection is necessitated, fast ions probably play a role by affecting the edge stability and, thus, ELMs.

The main difference between co-injected and counter-injected neutral beams is in the radial direction of the orbit-drift immediately following the ionization: the counter-injected ions drift outwards causing prompt losses to the walls, but at the same time feeding high energy particles into the edge region. For the well-confined co-injected beam ions this does not happen. Thus, the most obvious difference is the much higher direct ion orbit loss current. It would be tempting to assume that the high poloidal rotation driven by the resulting torque would explain the appearance of the QH-mode instead of the H-mode. This is, however, in contradiction to the second prerequisite of QH-mode, the large outer gap [3]. Another possible explanation is that the co- and counter-injection lead to different edge fast ion distribution which affects the edge MHD behaviour.

Earlier the difference between co- and counter-injected neutral beams has been studied using the orbit-following Monte Carlo code ASCOT [4]. The effects of toroidal ripple and typical QH-mode radial electric field E_r were taken into account, but the emphasis was more on the surface loads than on the fast ion distribution. Moreover, a programming error affecting the particle collisions made the effect of the radial electric field on the fast ion distribution seem insignificant, although it did not affect the conclusions about surface loads very much [5].

Here we revisit the fast ion edge distribution focusing on the differences between co- and counter-injections, corresponding to the H-mode and the QH-mode, respectively. The effects of a radial electric field and of a realistic toroidal ripple are taken into account. First, the simulation set-up is described in section 2, and the following section is dedicated to single-particle orbits of co- and counter-injected NBI ions both in the presence and in the absence of E_r. Finally, the modelling results on the distribution of NBI ions in the edge region are discussed. It is shown that there are differences in the fast ion distribution both in the configuration and in the velocity space between co- and counter-injected neutral beams. These differences could contribute to the different edge stability properties for the H-mode and the QH-mode.

2. The simulations

The steady-state slowing-down distribution of NBI-generated fast ions in the ASDEX Upgrade edge was simulated using the ASCOT code [6]. The plasma background and the magnetic equilibrium for the simulations were extracted from the ASDEX Upgrade database for the QH-mode discharge #17695 at $t = 5.6$ s. The global parameters of the discharge are listed in table 1. The direction of the ∇B-drift in the discharge was upwards. The temperature and density profiles and the q-profile used in the simulations are shown in figure 1 as a function of the normalized poloidal radius ρ_{pol} (=square root of normalized poloidal flux). A vacuum background was assumed for the scrape-off layer.

An ensemble of 9965 test particles was created using the FAFNER code [7] to represent two counter-injected neutral beams with 2.5 MW of nominal power each. The shine-through was taken into account in the FAFNER code, and the resulting absorbed power carried by the test particles was 4.9 MW corresponding to a source rate of $S_{\mathrm{NBI}} = 7.5 \times 10^{20}\,\mathrm{s}^{-1}$. Full (60 keV), half (30 keV) and one-third (20 keV) energy components were present in the ensemble. The power ratio of the energy components was 65 : 25 : 10 corresponding to a source rate ratio of

Table 1. Global plasma parameters for the ASDEX Upgrade QH-mode discharge #17695.

Plasma current	$I_\mathrm{p} = -1.0\,\mathrm{MA}$ (clockwise)
Toroidal magnetic field at geometric centre	$B_\mathrm{T} = 2.0\,\mathrm{T}$ (counter-clockwise)
Major and minor plasma radii	$R_0 = 1.65\,\mathrm{m}$, $a = 0.5\,\mathrm{m}$
Elongation	$\kappa = 1.71$
Upper and lower triangularities	$\delta_\mathrm{u} = 0.061$, $\delta_\mathrm{l} = 0.423$

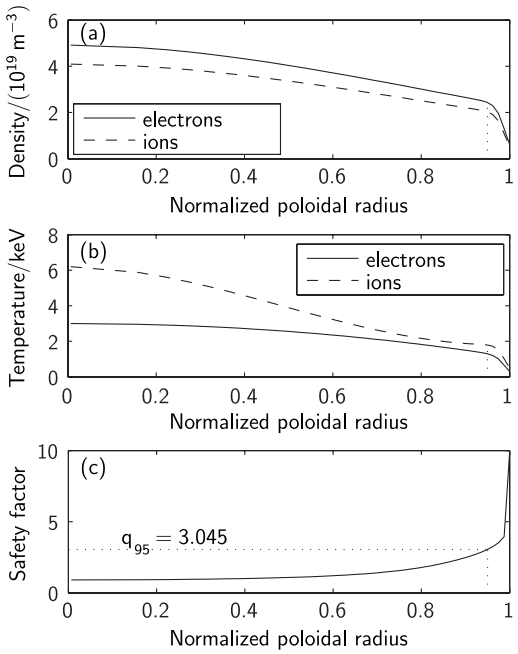

Figure 1. Plasma profiles for the ASDEX Upgrade QH-mode discharge #17695 at $t = 5.6\,\mathrm{s}$: (*a*) density, (*b*) temperature and 2(*c*) q-profile. In the first two the full (——) and dashed lines (- - - -) correspond to electrons and ions, respectively. The effective charge number is $Z_\mathrm{eff} = 2$ and 4% of carbon is assumed in the plasma. The pedestal (· · · · · ·) is roughly at $\rho_\mathrm{pol} = 0.95$.

44 : 35 : 21. The deposition profile of the beam ions as a function of the poloidal radius is shown in figure 2, and the initial pitch angle distribution in figure 3. The test particles were followed until their energy dropped below twice the local ion temperature T_i.

For comparison with co-injection, a virtual H-mode discharge was used instead of a real one so as to minimize the number of factors involved in the comparison. The virtual discharge was created from the real QH-mode data by reversing the plasma current, the toroidal magnetic field and the test particle pitch. As a result, also the direction of the ∇B-drift changed.

Four simulation set-ups with different combinations of magnetic ripple and radial electric field were applied both to the original QH-mode discharge and to the virtual H-mode discharge:

(1) no magnetic ripple, no radial electric field,
(2) no magnetic ripple, typical QH-mode radial electric field,
(3) finite toroidal ripple, no radial electric field and
(4) both finite toroidal ripple and typical QH-mode radial electric field.

The first two cases are idealized ones, present only in theory and modelling. A radial electric field is always present in experiments, but in some instances it is negligible, so that both the

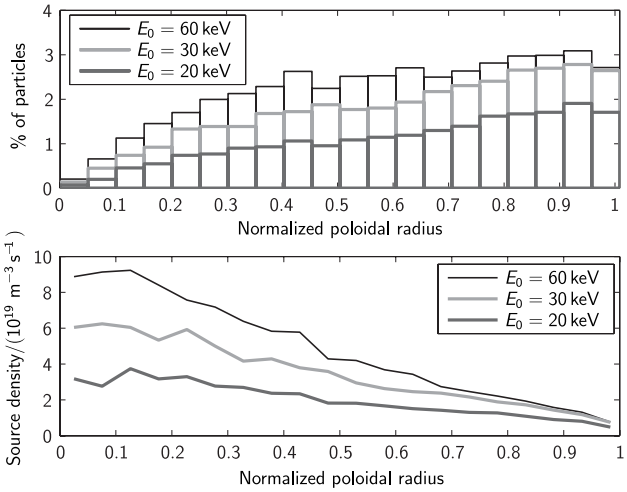

Figure 2. The deposition profiles of the full (60 keV), half (30 keV), and one-third (20 keV) energy components of the neutral beams. The upper figure is a histogram of particle percentages in normalized poloidal radius, and in the lower figure the corresponding source density is shown.

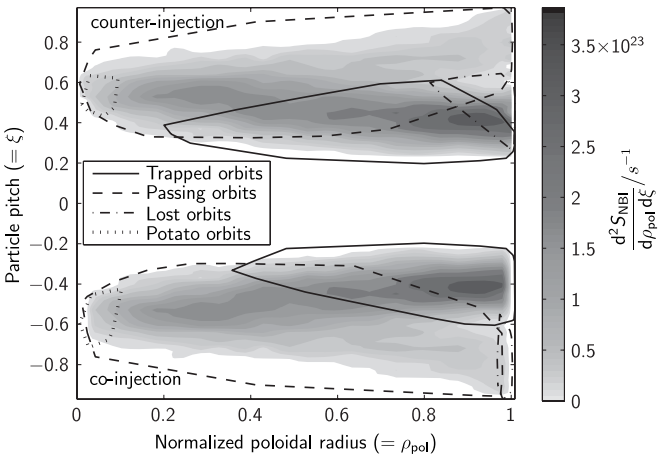

Figure 3. The initial pitch angle distribution of counter- (positive pitch axis) and co-injected (negative pitch axis) test particles. The latter is a mirror image of the former. The encircled regions in the figure correspond to the collisionless behaviour of the test particles (see section 3 for details). The regions overlap because the boundaries depend not only on the particle pitch and the normalized poloidal radius, but also on the poloidal angle.

latter two cases relate to the real world. The ripple map was obtained from vacuum field calculations. The ripple magnitude and the ripple-well region are shown in figure 4. The edge perpendicular velocity $u_\perp$-profile measured from the QH-mode discharge #16 111 by Doppler reflectometry [8] was used to calculate the radial electric field E_r profile shown in figure 5. The simplified expression for the radial electric field is $E_r = u_\perp B$. The justification for the simplification (neglecting the phase velocity in $u_\perp = v_{\boldsymbol{E}\times\boldsymbol{B}} + v_{\text{phase}}$, which allows one to interpret $u_\perp$ directly as the E_r profile) is presented in [8]. The same E_r profile was used in the simulations of both the real QH-mode discharge and the virtual H-mode discharge, again to keep the comparison as simple as possible.

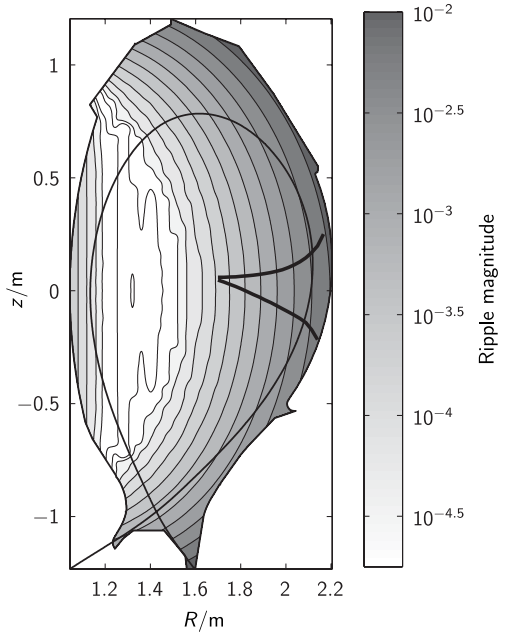

Figure 4. Contour plot of the ripple magnitude ($=\delta = (B_{\phi,\max} - B_{\phi,\min})/(B_{\phi,\max} + B_{\phi,\min})$) of the ASDEX Upgrade vacuum field. The ripple-well region is indicated in the figure by the thick lines, and also the separatrix of the QH-mode discharge #17695 at $t = 5.6$ s is shown.

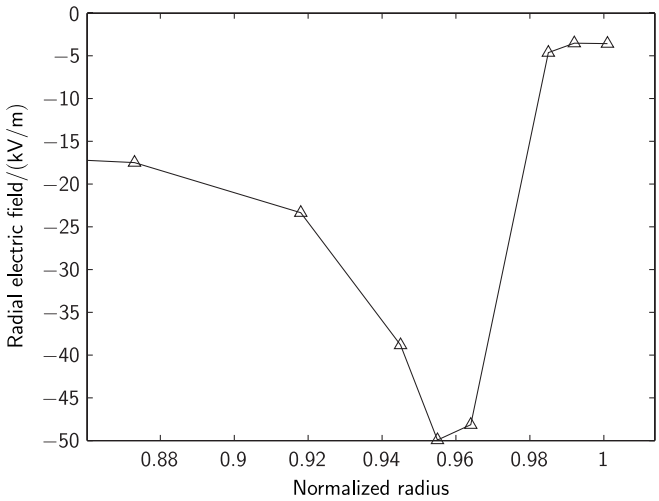

Figure 5. The radial electric field E_r profile used in the simulations. The profile was calculated from the edge perpendicular velocity $u_\perp$ profile measured from the ASDEX Upgrade counter-NBI discharge #16 111 by Doppler-reflectometry during QH-mode operation [8]. Inwards of the shown region, E_r was assumed to reduce linearly to zero at the magnetic axis.

In the simulations, in addition to the ripple and the radial electric field, the test particles experienced neoclassical transport modelled by Monte Carlo collision operators. Anomalous transport was neglected, but it is known to be at least partially suppressed in the H-mode edge region, and especially for fast ions its role is not significant. In order to obtain statistics, each

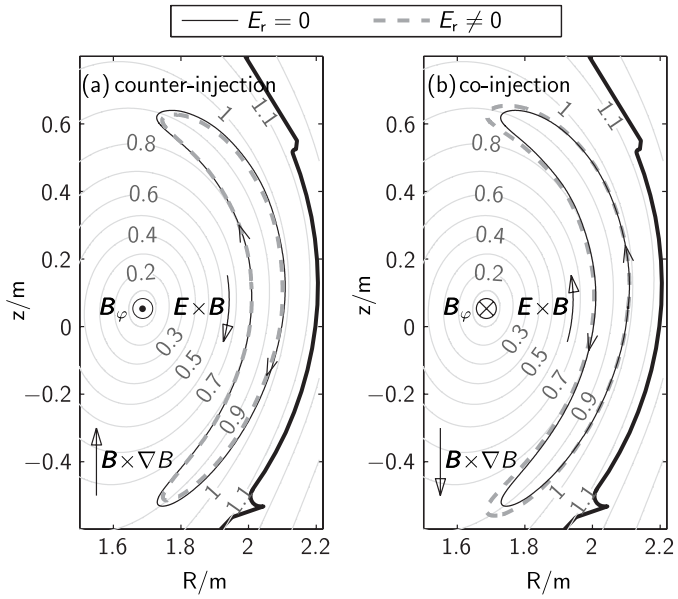

Figure 6. The effect of E_r shown in figure 5 on (*a*) a counter-injected, (*b*) a co-injected NBI ion. Also the directions of the toroidal magnetic field and the gradient and $\boldsymbol{E}\times\boldsymbol{B}$-drifts are shown. The counter-injected ion was initialized at $\rho_0 = 0.8$, $\theta_0 = 0^\circ$ with particle pitch $\xi_0 = 0.4$, and the co-injected ion at $\rho_0 = 0.98$, $\theta_0 = 0^\circ$ with particle pitch $\xi_0 = -0.4$. Both ions had initial energy of $E_0 = 60$ keV, and their pitches correspond to the injection direction of the neutral beams. With E_r the orbit of the counter-injected ion is squeezed, while the orbit of the co-injected ion is widened.

simulation set-up was repeated 10 times with different seeds of the pseudorandom number generator. This way, the sequence of pseudorandom numbers was different in each simulation and, thus, the test particles experienced different sequences of Monte Carlo collisions. The final results were obtained by averaging the results of the 10 sub-simulations. Also the standard deviations were calculated.

3. Collisionless orbits

Before going into the results of full simulations it is informative to discuss collisionless single-particle orbits. Figure 6 shows the orbits of typical counter- and co-injected ions in the poloidal cross-section with and without radial electric field. Also shown in the figure are the directions of the gradient and $\boldsymbol{E}\times\boldsymbol{B}$-drifts, which point to the opposite directions for co- and counter-injections. Figure 7 shows the time evolution of the particle pitch for the same orbits. To facilitate the comparison, the initial conditions were chosen such that the co- and counter-injected orbits match in the absence of E_r.

The counter-injected ion moves outwards on its first half-orbit after ionization due to the upward-pointing ∇B-drift. Conversely, the co-injected ion first drifts inwards due to the downward ∇B-drift, which is why the orbits of co-injected ions are generally called well confined. A common feature of co- and counter-injected orbits is that the duration of the outer leg of the orbit corresponding to the negative particle pitch is longer than the duration of the inner leg corresponding to the positive particle pitch (see figure 7). This is because the ions need to move farther in the toroidal direction on the outer leg than on the inner leg of their orbits due to the monotonically increasing q-profile (see figure 1). This is, however, not

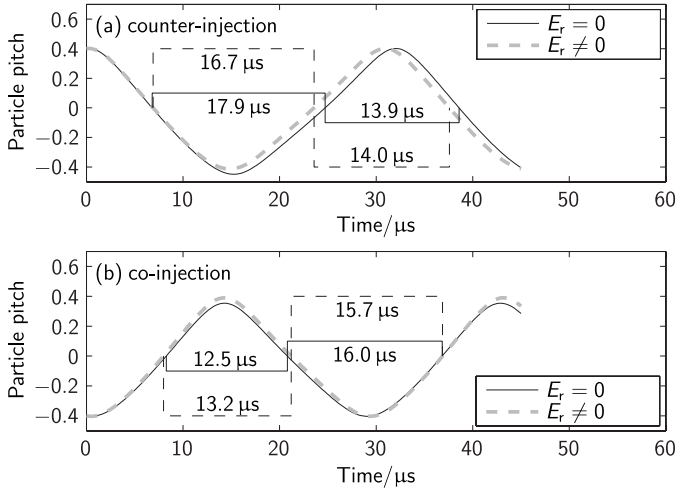

Figure 7. The time evolution of the particle pitch and the durations of the outer and the inner legs for the orbits shown in figure 6. For both counter- and co-injection the outer leg of the orbit with negative pitch is longer, both in time and in space, than the inner leg with positive pitch. With non-zero E_r, however, the $\boldsymbol{E} \times \boldsymbol{B}$-drift pointing to the direction of negative parallel velocity (see figure 6), decreases (increases) the duration of the outer (inner) leg. As a result, the asymmetry in the duration of the inner and the outer legs is decreased for both counter- and co-injections.

self-evident, because the parallel velocity increases with increasing major radius which shortens the time spent on the outer leg.

Next we discuss the effect of the radial electric field, which conventionally is thought to be the orbit-squeezing arising solely from the gradient of E_r [9]. However, for single ions also a constant E_r can cause orbit-squeezing or *widening* depending on the injection direction [1]. This is because radially outward-drifting (inward-drifting) trapped ions lose (gain) kinetic energy when they move towards increasing (decreasing) electric potential. Consequently the turning points of counter-injected (co-injected) ion orbits move towards smaller (larger) major radius thereby decreasing (increasing) the time the ions experience the upward (downward) ∇B-drift. This movement of the turning points can be seen in figure 6. The resulting squeezing of the counter-injected orbit and widening of the co-injected orbit is less apparent in the figure, but it can be verified by plotting the normalized poloidal radius as a function of time (not shown). Another effect is the decrease (increase) of the duration of the outer (inner) leg of the orbit, shown in figure 7. This is due to the $\boldsymbol{E} \times \boldsymbol{B}$-drift which points to the direction of negative $v_\parallel$ for both injection directions. Thus, in both cases the radial electric field reduces the asymmetry in the duration of the outer and the inner legs of the orbit.

The collisionless orbits of all 9965 test particles in the full ensembles were also simulated both in the absence and in the presence of E_r. The orbit topologies were then analysed and divided into three categories: trapped, untrapped and first orbit loss. A detailed breakdown, also as a function of initial energy, is shown in tables 2 and 3, and regions in the phase space corresponding to each category are shown in the initial pitch distribution in figure 3. In the figure, the untrapped orbits are further divided into passing and potato orbits. The trapped orbits were further analysed to find out the orbit widths and the duration of the inner and the outer legs of the orbits, and the results verify the above findings: with only a few exceptions the radial electric field squeezes the counter-injected orbits and widens the co-injected orbits. Likewise, the asymmetry in the duration of the outer and the inner legs is consistently reduced.

Table 2. The breakdown of co-injected particle orbits into trapped, untrapped and lost for all initial energies and both in the absence and presence of E_r.

	Percentage trapped		Percentage untrapped		Percentage lost	
Initial energy (keV)	$E_r = 0$	$E_r \neq 0$	$E_r = 0$	$E_r \neq 0$	$E_r = 0$	$E_r \neq 0$
60	16.91	16.50	26.51	26.91	0.45	0.45
30	17.46	16.97	17.25	17.74	0.08	0.08
20	11.87	11.32	9.42	9.97	0.05	0.05
All	46.24	44.79	53.18	54.62	0.58	0.58

Table 3. The breakdown of counter-injected particle orbits into trapped, untrapped and lost for all initial energies and both in the absence and presence of E_r.

	Percentage trapped		Percentage untrapped		Percentage lost	
Initial energy (keV)	$E_r = 0$	$E_r \neq 0$	$E_r = 0$	$E_r \neq 0$	$E_r = 0$	$E_r \neq 0$
60 keV	18.70	19.39	21.22	20.84	3.95	3.64
30 keV	19.08	19.77	13.85	13.35	1.86	1.68
20 keV	13.14	13.69	7.48	7.02	0.71	0.62
All	50.92	52.85	42.55	41.21	6.52	5.94

Table 4. The percentage of orbits undergoing a transition when E_r is switched on. Let us denote the set of particles with orbit topology A and initial energy E_0 by $S_A(E_0)$. Then the percentages shown can be defined as $\#\{S_A(E_0) \cap S_B(E_0)\}/\#S_A(E_0)$, where A and B are the initial ($E_r = 0$) and final ($E_r \neq 0$) orbit topologies, respectively. Because of this definition, the percentages of individual energies do not add up to the percentage of all energies, or 100%.

	Co-injection	Counter-injection	
Initial energy (keV)	Trapped → Untrapped (%)	Untrapped → Trapped (%)	Lost → Trapped (%)
60	2.38	1.80	7.91
30	2.82	3.63	9.72
20	4.63	6.14	12.64
All	3.12	3.16	8.95

From table 2 it can be seen that for co-injection, the fraction of trapped orbits is decreased and the fraction of untrapped orbits increased when the radial electric field is switched on. For the counter-injection the effect is reversed, as can be seen in table 3. Also the fraction of lost particles is decreased for counter-injection. In table 4 this transition in orbit topology is analysed in more detail.

4. Edge fast ion distribution

Equipped with insight gained from the single-particle simulations we now turn our attention to the full simulations. The following distributions were obtained:

Radial density. Flux-surface averaged fast ion ($E \geqslant 2\,T_i$) density as a function of the normalized radius ρ_{pol}, figure 8.

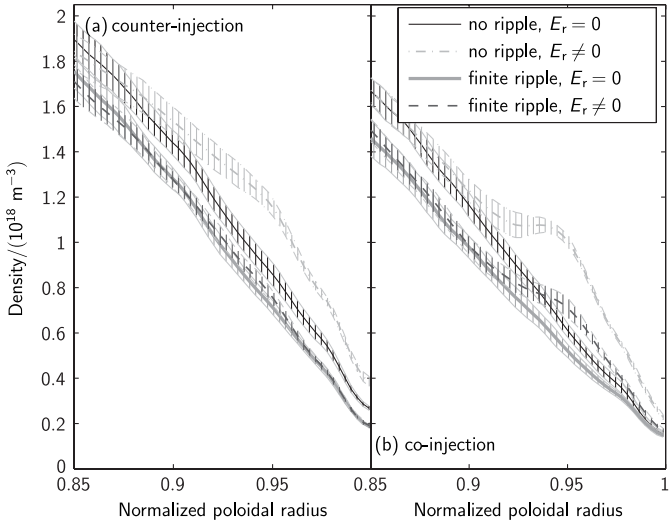

Figure 8. The flux-surface averaged fast ion density as a function of normalized radius ρ_{pol} in (*a*) counter-injection and (*b*) co-injection simulations. The 95% confidence intervals (2 standard deviations) are indicated by the error bars.

Energy distribution. Fast ion phase space density as a function of ρ_{pol} and energy E, figures 9–12.

Pitch angle distribution. Fast ion phase space density as a function of ρ_{pol} and particle pitch ξ, figures 13–16.

4.1. Radial density

Figure 8 shows the radial density from all four simulations of (*a*) counter-injected and (*b*) co-injected neutral beams corresponding to the real QH-mode and the virtual H-mode, respectively. The fast ion density in the edge pedestal region ($\rho_{\mathrm{pol}} \approx 0.95$) is higher and the density gradient steeper for the counter-injected ions. This can be explained by the low ionization probability near the edge and the difference in the orbits of co- and counter-injected ions discussed above (see also figure 6). Regardless of the injection direction only a few particles are ionized near the separatrix. The co-injected ions are well confined, but most of the counter-injected particles ionized near the separatrix are promptly lost to the walls. However, the ionization probability increases with decreasing ρ_{pol} so that more particles are ionized farther inside the plasma. With counter-injection, the orbits of these ions extend to the edge thus increasing the fast ion density compared with the co-injection case there.

The effect of the ripple is to reduce the density throughout the region shown in figure 8 except for co-injected ions at the very edge of the plasma. Also for the counter-injected ions the density reduction is smaller close to the separatrix. Consequently the ripple reduces the fast ion density gradient in both cases.

The radial electric field, on the other hand, increases the density especially near $\rho_{\mathrm{pol}} \approx 0.94$, which is the region of strongest gradient in the radial electric field inward of its maximum point at $\rho_{\mathrm{pol}} \approx 0.955$. The squeezing and widening of the counter- and co-injected orbits probably also plays a role, but the most likely explanation for the increased density is the E_r-induced orbit transformations. For co-injection, marginally trapped particles initialized

near $\rho_{\rm pol} \approx 0.95$ are transformed into untrapped particles, which greatly decreases their orbit width. For counter-injection marginally *untrapped* particles initialized deeper in the plasma are transformed into wide trapped orbits which extend outwards to $\rho_{\rm pol} \approx 0.95$. This becomes clearer later when we discuss the pitch distributions. The overall effect in both cases is increased fast ion density, and increased (decreased) density gradient outward (inward) of $\rho_{\rm pol} \approx 0.94$.

With counter-injection, including simultaneously the effects of both the ripple and the radial electric field has no significant effect on the fast ion density compared with the case with only ripple. For co-injected ions the effect of E_r together with the ripple is much stronger. In the region $\rho_{\rm pol} > 0.93$ the density is even higher than in the ideal case without either ripple or E_r, and also the gradient is closer to that with E_r.

4.2. Energy distribution

Having discussed the fast ion distribution in the configuration space we next move on to the fast ion slowing-down distribution in the velocity space. The energy distributions obtained from the simulations are shown in figures 9–12. Figures 9 and 10 correspond to counter-injection and figures 11 and 12 to co-injection. The idealized cases without ripple are shown in figures 9 and 11, and the cases with finite toroidal ripple in figures 10 and 12. The injection energies 60, 30 and 20 keV show clearly in all figures as folds of the contour lines, which are simply discontinuities in the first derivative with respect to energy caused by the delta-function particle source. Above the full injection energy the density quickly diminishes to zero because there is little upscattering at that energy.

The effect of the ripple, the decreased phase space density, appears in figures 10(*a*) and 12(*a*) as contour lines receding to smaller normalized radii compared with the figures 9(*a*) and 11(*a*), in accord with the situation depicted in figure 8. Similarly, the increased density and density gradient caused by the radial electric field show as contour lines agglomerating at the edge region $\rho_{\rm pol} > 0.95$ in figures 9(*b*) and 11(*b*). The density changes are also reflected in the tones of grey. The local maximum of the co-injected fast ion density observed in figure 8(*b*) is also visible in figure 11(*b*) at energies around $E \approx 15$ keV. The fast ion distributions under the combined effect of both the ripple and the E_r, shown in figures 10(*b*) and 12(*b*), are close to the ideal cases in figures 9(*a*) and 11(*a*).

4.3. Pitch distribution

Figures 13–16 show the pitch angle distributions. For energy distributions, figures 13 and 14 correspond to counter-injection and figures 15 and 16 to co-injection. Also the arrangement of the figures with respect to the ripple is the same. In each counter-injection figure, the ions created on the untrapped orbits appear as a protrusion in the region $\xi > 0.6$. For co-injection, there is a similar protrusion from untrapped ions orbiting in the opposite direction. However, there is a difference in the radial extent of these protrusions stemming from the different directions of the gradient drift. For co-injection, the untrapped particle population stretches all the way to the separatrix, but it is somewhat masked because the distribution on the whole leans to the negative ξ side. Indeed, for both co- and counter-injections the majority of the particles in the distribution have negative pitch. This is as expected, since the ions spend more time on the outer legs of their orbits as discussed above and illustrated in figure 7. The equalizing effect of the $\boldsymbol{E} \times \boldsymbol{B}$-drift (time- and orbit-leg-wise) shows especially well in figures 13(*b*) and 15(*b*), but also in the corresponding figures with ripple.

The orbit-transition effect mentioned above clearly shows in figures 13(*b*) and 15(*b*). In figure 13(*b*), the phase space density is reduced in the upper part of the figure ($\xi > 0.6$)

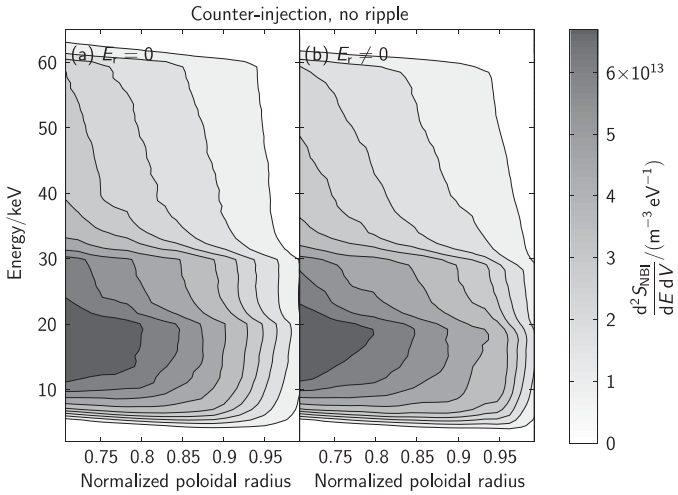

Figure 9. The energy distribution of counter-injected fast ions in axisymmetric magnetic field (*a*) without E_r and (*b*) with E_r of figure 5.

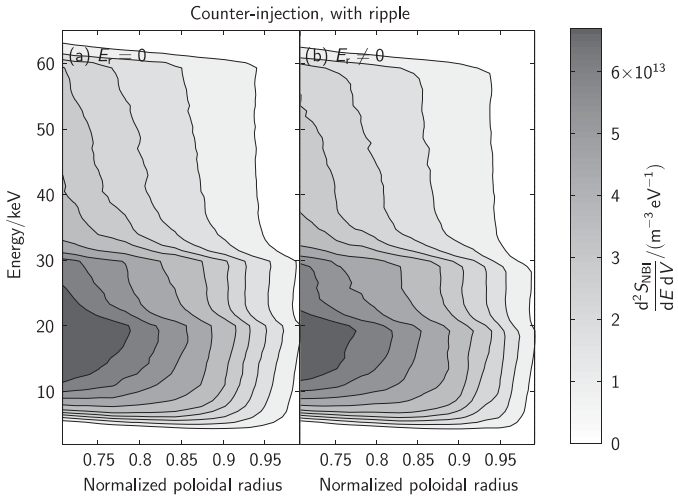

Figure 10. The energy distribution of counter-injected fast ions in the presence of ripple (*a*) without E_r and (*b*) with E_r of figure 5.

corresponding to untrapped particles and increased in the middle. The collisionless orbit transitions in table 4 are probably not enough to account for the change in the distribution, but it is likely that also more orbits undergo transition after the particles have slowed down first. In figure 15(*b*), the distribution is 'hollowed' around $(\rho, \xi) = (0.9, -0.7)$ and the initially trapped particles in this region have become untrapped particles at roughly $(\rho, \xi) = (0.95, -0.8)$. The same seems to have happened for counter-injected particles too in figure 13(*b*), but in this case they must be particles which have undergone pitch angle scattering first, because for counter-injection there are no particles initialized into this region of phase space.

The effect of ripple alone shows near $\xi = 0$ as concavity of the contour lines (see figures 14(*a*) and 16(*a*), and to a lesser extent when electric field is also present. This means

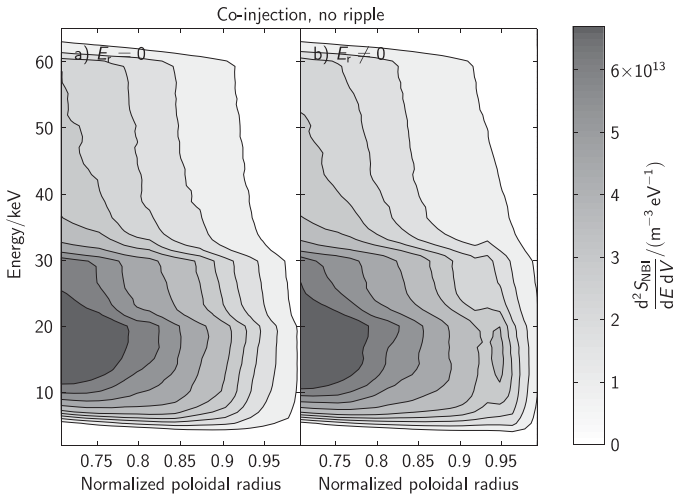

Figure 11. The energy distribution of co-injected fast ions in axisymmetric magnetic field (*a*) without E_r and (*b*) with E_r of figure 5.

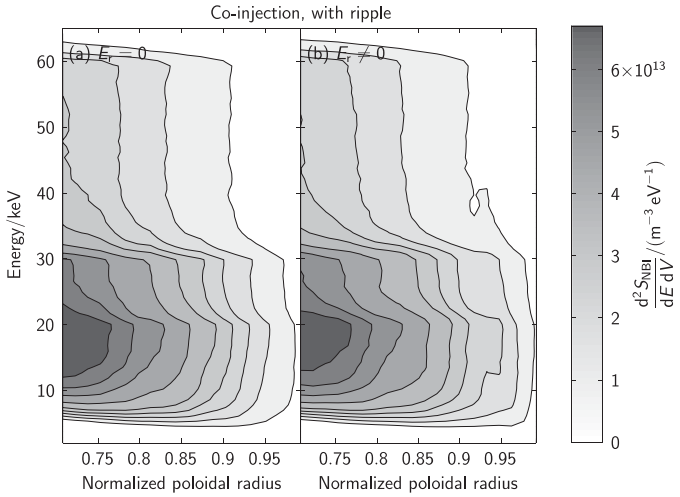

Figure 12. The energy distribution of co-injected fast ions in the presence of ripple (*a*) without E_r and (*b*) with E_r of figure 5.

that part of the ions having small pitch have been removed from the distribution. The 'island' of untrapped particles at $(\rho, \xi) = (0.95, -0.8)$ has survived in figure 16(*b*), but in figure 14(*b*) the E_r-effects are mostly missing. In both cases the ripple-induced stochastic diffusion and particle losses due to ripple-trapping weaken the effect of E_r considerably, and figures 14(*b*) and 16(*b*) are similar to the corresponding ideal cases in figures 13(*a*) and 15(*a*).

5. Conclusions and discussion

The edge fast ion distribution of co- and counter-injected neutral beam ions in ASDEX Upgrade has been studied by ASCOT simulations. The effects of radial electric field and finite toroidal

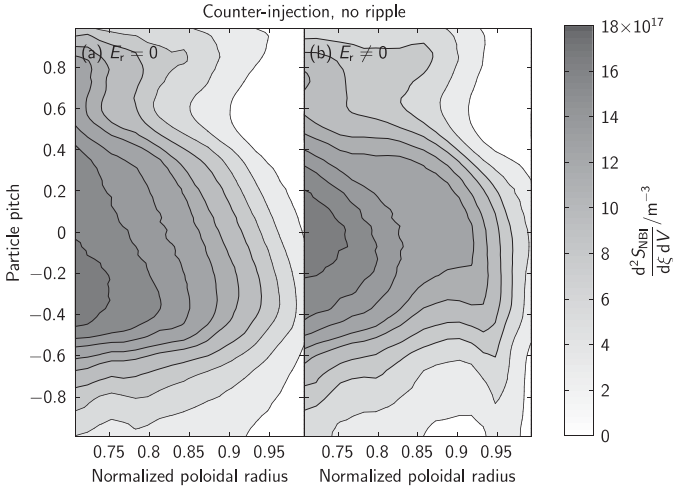

Figure 13. The pitch angle distribution of counter-injected fast ions in axisymmetric magnetic field (*a*) without E_r and (*b*) with E_r of figure 5.

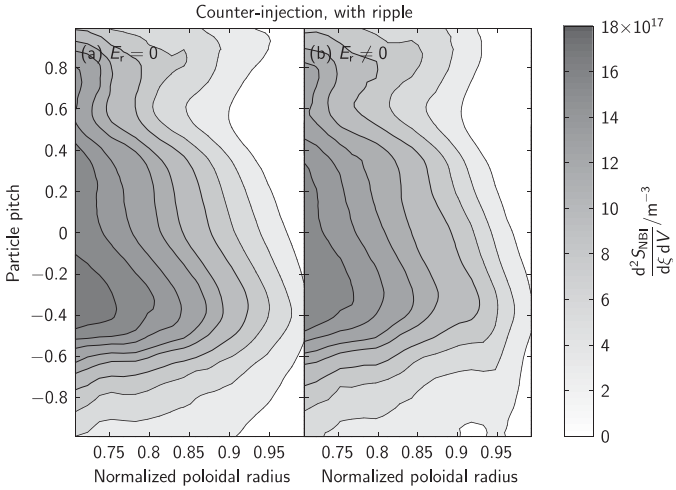

Figure 14. The pitch angle distribution of counter-injected fast ions in the presence of ripple (*a*) without E_r and (*b*) with E_r of figure 5.

ripple were taken into account. Also the collisionless single-particle orbits of both injection directions and the effect of radial electric field on them were analysed.

The overall finding about the edge fast ion distribution is that the fast ion density and its gradient in the pedestal region are higher for counter-injection than for co-injection. With counter-injection, ions born farther inside the plasma are fed into the edge region (or onto the walls), while for co-injection the few particles ionized in the edge region spend most of their time inward of the ionization point on their well-confined orbits. However, the differences are not limited just to the number of ions in the edge region, but also their distribution in the velocity space is different. For co-injection, a population of untrapped particles exists at the edge, and it becomes especially pronounced in the presence of a radial electric field. For

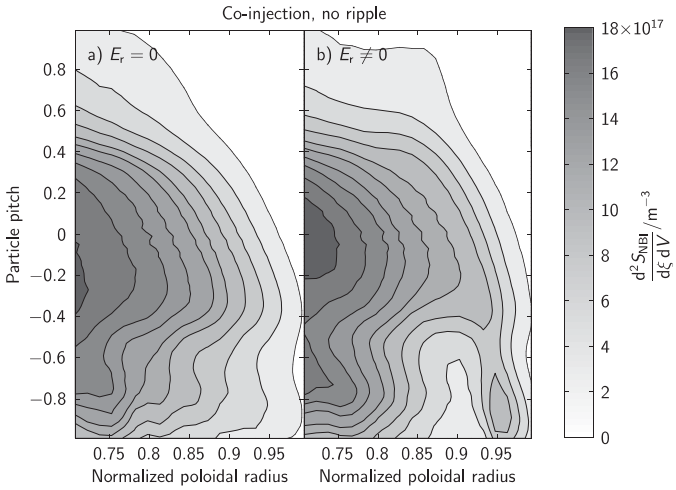

Figure 15. The pitch angle distribution of co-injected fast ions in axisymmetric magnetic field (*a*) without E_r and (*b*) with E_r of figure 5.

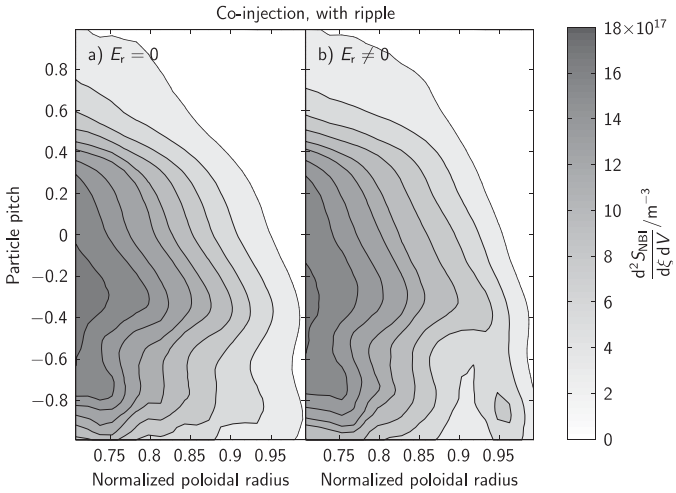

Figure 16. The pitch angle distribution of co-injected fast ions in the presence of ripple (*a*) without E_r and (*b*) with E_r of figure 5.

counter-injection, such a population exists only with non-zero E_r and even then it is much weaker than for co-injection. These differences may well have implications on the different MHD behaviour between the H-mode and the QH-mode.

The toroidal ripple reduces the fast ion density and also its gradient by removing particles with low pitch. In the pitch angle distributions this shows as concavity of the contour lines near $\xi = 0$. However, including simultaneously the effects of both the ripple and the radial electric field seems to restore the fast ion distribution closer to the ideal case where both of them are absent. This is a useful result for modelling purposes since the usual assumption of axisymmetry does not necessarily mean the result is far from reality, at least in the co-injection/H-mode case.

The radial electric field increases the edge density and density gradient for both injection directions. The effect is most prominent in the vicinity of the maximum point of the E_r profile, especially for co-injection. The pitch angle distributions suggest that the density increase is in both cases mostly due to transitions between the trapped and the untrapped orbits.

Since the input data for the co-injection simulations were created from real QH-mode and counter-injection data, the results obtained about co-injection do not necessarily relate directly to real H-mode discharges. However, the result about the lower fast ion density at the edge for co-injection is probably true because in a real H-mode there are two factors which would make the edge fast ion density even lower compared with QH-mode: the ionization rate of beam ions at the edge would be lower due to lower edge density, and the effect of E_r increasing the fast ion density would be weaker due to weaker E_r H-mode.

The non-constant radial electric field typical of a QH-mode is found to squeeze the orbit of a counter-injected NBI ion but to widen the orbit of a co-injected beam ion. This is in contrast to the conventional wisdom according to which only the E_r gradient can change the orbit width and the effect is always orbit-squeezing. The radial electric field is also found to decrease the asymmetry in the duration of the inner and the outer legs of the trapped particle orbits caused by the monotonically increasing q-profile. This is in line with the earlier finding that a constant, negative radial electric field reduces the toroidal precession or even reverses it [1]. Probably the most important E_r-effect on particle orbits, however, is the transition of marginally trapped orbits into untrapped ones for co-injection and the converse effect for counter-injection. Both the orbit squeezing/widening and orbit transitions have an effect on the neoclassical transport, but since trapped-to-untrapped pairs with orbit-widening for co-injection and the opposite happens for counter-injection, the two are always opposing each other.

Acknowledgments

This work, supported by the European Communities, under the contract of Association between Association Euratom/Tekes, was carried out within the framework of the European Fusion Development Agreement. The views and opinions expressed herein do not necessarily reflect those of the European Commission. The computations presented in this document have been made with CSC's computing environment. CSC is the Finnish IT centre for science and is owned by the Ministry of Education.

References

[1] Suttrop W *et al* 2005 *Nucl. Fusion* **45** 721–30
[2] Burrell K H *et al* 2002 *Plasma Phys. Control. Fusion* **44** A253–63
[3] Suttrop W *et al* 2003 *Plasma Phys. Control. Fusion* **45** 1399–416
[4] Hynönen V, Kurki-Suonio T, Suttrop W, Dux R, Sugiyama K and the ASDEX Upgrade Team 2007 *Plasma Phys. Control. Fusion* **49** 151–74
[5] Hynönen V and Kurki-Suonio T 2007 *Plasma Phys. Control. Fusion* **49** 1345–7
[6] Heikkinen J A and Sipilä S K 1995 *Phys. Plasmas* **2** 3724–33
[7] Lister G G 1985 *Technical Report* 4/222 IPP Garching, Germany
[8] Conway G D, Schirmer J, Klenge S, Suttrop W, Holzhauser E and the ASDEX Upgrade Team 2004 *Plasma Phys. Control. Fusion* **46** 951–70
[9] Hazeltine R D 1989 *Phys. Fluids B: Plasma Phys.* **1** 2031–9